Structural and electronic properties of Xe

2000 J. Phys.: Condens. Matter 12 9869

(http://iopscience.iop.org/0953-8984/12/48/305)

J. Phys.: Condens. Matter **12** (2000) 9869–9883. Printed in the UK PII: S0953-8984(00)16030-8

Structural and electronic properties of Xe

Michael Springborg†
Department of Chemistry, University of Konstanz, 78457 Konstanz, Germany
E-mail: m.springborg@mx.uni-saarland.de

Received 2 August 2000

Abstract. Using different density-functional methods, dimers, chains, monolayers, and crystals of Xe are studied. In contrast to most of the earlier studies on crystalline Xe, this one concentrates on structures with expanded lattices compared with equilibrium. In order to make a comparison with experimental photoelectron information, the variation of the band structures and density of states with distance is analysed in detail. Here, the calculations give results that are mutually consistent and in agreement with some other theoretical works, but which show some differences from other theoretical and some experimental studies. The differences that are observed for chains and monolayers, which experimentally are produced on some substrate, may be due to substrate–Xe interactions. In addition, we explore how spin–orbit couplings influence the results, and the differences between using a local-density and a generalized-gradient approximation are studied. For those systems where other information on the optimized bond length exists it is found that the density-functional calculations are inaccurate. When a comparison is possible, the bonds are found to be too short. Moreover, the calculations predict in all cases the existence of stable structures.

1. Introduction

Artificially produced systems of lower dimensions are becoming increasingly important both for applications in new electronic and optical devices and for basic research since the reduced dimensions often lead to special quantum-confinement effects. In some cases, such systems are produced as free-standing objects but in most cases they are deposited on some substrate. In that case the substrate may dictate the structure of the deposited system, but may also modify the properties of the latter in an uncontrolled manner. One way of reducing the importance of these interactions is to consider materials for which they are by definition small, e.g., inert gases.

Xe is one of the inert gases. It is, however, less inert than others of the group VIII of the periodic table, which can, e.g., be quantified through the van der Waals constants a and b. These are $a = 0.034$, 0.21, 1.35, 2.32, and 4.19 l^2 atm mol^{-2} and $b = 0.024$, 0.017, 0.032, 0.040, and 0.051 l mol^{-1} for He, Ne, Ar, Kr, and Xe, respectively [1], i.e., clearly largest for Xe. Therefore, it is believed that, when depositing Xe atoms on some substrate, the interactions between the substrate and the Xe atoms are so strong that well-ordered structures of Xe can be obtained but, on the other hand, not so strong that they interfere with the Xe–Xe interactions.

By depositing Xe atoms on different surfaces it has become possible to produce ordered two-dimensional layers [2, 3] and, more recently, also one-dimensional chains [4–7]. Often, the materials are characterized through photoelectron spectroscopy experiments that through comparison with theoretical studies can be interpreted. The theoretical studies consider most often only a single geometry (i.e., the one that is experimentally relevant) and treat either an isolated film or chain or, alternatively, the substrate with the adsorbed Xe atoms. There has

† Present address: Physical Chemistry, University of Saarland, 66123 Saarbrücken, Germany.

0953-8984/00/489869+15$30.00

been, however, no systematic study of the effects of changing the dimensionality and/or the interatomic distances, although such a study is very important when seeking to identify those experimental signals that are due to Xe–Xe interactions and those that are due to Xe–substrate interactions. Moreover, more seriously, there are some discrepancies between the different experimental and theoretical studies of the band structures for one- and two-dimensional Xe systems that have not been resolved.

It is the purpose of the present communication to provide the results of a such study. We shall use four different density-functional methods in studying a Xe atom, a Xe_2 dimer, an infinite Xe chain, an infinite Xe monolayer, and an infinite Xe crystal. Although clusters of Xe have also been produced [8], these have not been included in our study. We shall concentrate on the optimized bond length for the different structures as well as on how the electronic interactions change as a function of interatomic distance and of structure. Furthermore, since the interatomic interactions of Xe are weak, they may be difficult to treat theoretically and we shall therefore also explore how they are described with the different computational schemes, including studying how they depend on whether spin–orbit couplings are included and on whether a local-density approximation (LDA) or a generalized-gradient approximation (GGA) within the density-functional formalism is used.

There have been a number of experimental and theoretical studies devoted to crystalline xenon, aimed in particular at exploring a pressure-induced transition to a metallic state [9–16]. Accordingly, in those studies compressed structures were examined. Here, however, we study expanded structures with nearest-neighbour distances similar to those of the experimental studies of Xe monolayers and chains deposited on some substrate. This means also that the experimentally studied systems are far from being metallic.

The outline of the paper is as follows. In section 2 we describe the computational methods briefly. Section 3 contains the results, and the conclusions are summarized in section 4.

2. Computational methods

We apply the density-functional formalism of Hohenberg and Kohn [17]. In the formulation of Kohn and Sham [18] the total energy is calculated by solving the single-particle equations

$$\hat{h}_{\mathrm{eff}}\psi_i(\vec{r}) = \epsilon_i\psi_i(\vec{r}) \tag{1}$$

with

$$\hat{h}_{\mathrm{eff}} = -\frac{\hbar^2}{2m}\nabla^2 + V(\vec{r}). \tag{2}$$

The potential is written as

$$V(\vec{r}) = V_{\mathrm{n}}(\vec{r}) + V_{\mathrm{C}}(\vec{r}) + V_{\mathrm{xc}}(\vec{r}) + V_{\mathrm{rel}}(\vec{r}) \tag{3}$$

i.e., as a sum of the Coulomb potential from the nuclei, that from the electrons, the exchange–correlation potential, and the relativistic correction. The latter,

$$V_{\mathrm{rel}} = -\frac{1}{8m^3c^2}\nabla^4 + \frac{1}{8m^2c^2}\nabla^2 V + \frac{1}{4m^2c^2}(-\mathrm{i}\,\vec{\nabla}V \times \vec{\nabla})\cdot\vec{s} \tag{4}$$

includes the mass–velocity term, the Darwin term, and the spin–orbit couplings. For an isolated atom the potential $V(\vec{r})$ of equation (3) is spherically symmetric and equation (1) can be solved numerically [19], which we did both when including relativistic effects and when excluding these (i.e., setting $c \to \infty$). In the scalar-relativistic calculations only the last term (the spin–orbit couplings) of equation (4) is excluded.

For any other system we expand the eigenfunctions ψ_i in a basis set of augmented waves that are defined as follows. We separate the three-dimensional space into atom-centred spheres

and the interstitial region. Inside any sphere a set of (numerical) functions $\{\phi\}$ is constructed by solving equation (1) numerically for chosen energies $\{\epsilon_\nu\}$. In addition, their derivatives $\{\dot{\phi}\}$ with respect to ϵ_ν are introduced. In the interstitial region we consider either spherical waves $h_l^{(1)}(\kappa|\vec{r}-\vec{R}|)Y_{lm}(\widehat{r-R})$ (where $h_l^{(1)}$ is a spherical Hankel function, $\vec{R}$ is the atom at which the function is centred, and κ is a purely imaginary decay constant), or plane waves $e^{i\vec{k}\cdot\vec{r}}$. These waves are augmented continuously and differentiably on the sphere boundaries with linear combinations of the numerically given functions $\{\phi\}$ and $\{\dot{\phi}\}$, i.e., as $\sum C(\phi+\omega\dot{\phi})$ with C and ω being some constants depending on $\vec{R}$, l, m, κ, and $\vec{k}$, and with the sum running over (l, m).

The WIEN programs [20] are based on the FLAPW (full-potential linearized augmented-plane-wave) method whereby plane waves are used as basis functions. Moreover, the spheres are non-overlapping and the full potential is used (i.e., not only its muffin-tin part that is used in the construction of the basis functions). These programs were here used in studying different crystalline materials, whereby monolayers and chains were also treated by separating the monolayers by 30 au and the chains by 15 au, respectively. The radii of the spheres were set equal to 3.0 au, and all but the 4d, 5s, and 5p electrons were considered core electrons (the WIEN programs allow for treating more orbitals as valence orbitals than is the case with the other programs, but since the 4d orbitals for an isolated atom appear at about −60 eV, the treatment of these as valence or core orbitals should make little difference). For the sake of completeness we add that the parameters $R_{MT}k_{max}$ and G_{max} that control the plane-wave expansions were set equal to 10 au (the latter to 12 au for the calculations on the crystalline systems), and the potential was expanded up to $l = 10$ inside the spheres. Finally, in the sampling of the $\vec{k}$-space we used only 10–20 points in the irreducible part of the first Brillouin zone since the systems are insulators with narrow bands.

In addition, the isolated dimer as well as isolated chains were studied using the full-potential (FP) LMTO programs for isolated, infinite, periodic chains [21,22]. These are based on the use of spherical waves (actually two functions for each atom and (l, m), differing in the decay constants κ). The dimers were treated by considering a chain of such entities separated by 200 au, and for the chains we used seven k-points in half of the first Brillouin zone. Moreover, the sphere radii were set equal to 2.2 au, and in these calculations also the 4d electrons were treated as core electrons.

Finally, we also used the LMTO-ASA programs [23]. Also here spherical waves are used as basis functions but the spheres are expanded so that they overlap slightly and so that their total volume equals that of the crystal. The effects of the overlaps and of the interstitial region are included perturbatively, and only the spherically symmetric parts of the potential are considered. Moreover, only one κ is used which is set equal to $\kappa = 0$. Also here the 4d electrons were considered as core electrons, and we used 20 $\vec{k}$-points in the irreducible part of the first Brillouin zone.

Since the interatomic interactions for the inert gases are so weak, it has been found to be difficult to describe these with current approximations to $V_{xc}(\vec{r})$ (see, e.g., [24]). As an extension of the study by Pérez-Jordá and Becke [24] we have therefore considered both local-density [25,26] and generalized-gradient [27,28] approximations.

3. Results

Starting with the isolated atom we shall gradually increase the dimensionality and size of the systems by subsequently considering dimers, chains, monolayers, and, ultimately, crystals. We shall concentrate on the optimized nearest-neighbour bond lengths as well as the electronic

interactions (e.g., positions and widths of the different bands) as functions of interatomic distances. To our knowledge, there exist only very few studies devoted to determining the optimal structure of Xe-based systems, i.e., some studies for Xe_2 and Xe_2^+ (see, e.g., [29–33]) as well as for crystalline Xe (see, e.g., [32]).

3.1. The isolated atom

For an isolated atom we find 4d levels at −61.00 and −59.00 eV, the 5s level at −20.42 eV, and 5p levels at −9.72 and −8.45 eV. Here, the splittings are due to the spin–orbit couplings. Setting $c \to \infty$ changes these numbers into −62.66, −18.75, and −8.88 eV for the 4d, 5s, and 5p levels, respectively. In these calculations we used a LDA. In comparison, Hartree–Fock calculations without relativistic effects have given −75.59, −25.70 eV, and −12.44 eV for the same three levels [34]. The Hartree–Fock eigenvalues being deeper and spanning a broader range than the density-functional eigenvalues is often seen.

3.2. The dimer

In table 1 we list the calculated equilibrium bond lengths for the different systems considered here. It is seen that the inclusion of spin–orbit couplings hardly affects the results for the dimer, but that LDA calculations give a smaller bond length than GGA calculations, which is often found. Experimentally, the bond length is 8.24 au [29, 31, 33], whereas correlated *ab initio* calculations [32] have given 8.33 au. Thus, the present calculations underestimate this value independently of whether a LDA or a GGA is used.

Table 1. Optimized nearest-neighbour bond lengths (in au) for different structures of Xe, i.e., the Xe_2 dimer, an infinite linear chain, a hexagonal monolayer, a square monolayer, and an FCC crystal. 'LDA' and 'GGA' mark results obtained with a local-density and a generalized-gradient approximation, and '−SOC' and '+SOC' indicate whether spin–orbit couplings are included. The different computational methods are distinguished through the acronyms of section 2.

System	Method	LDA, −SOC	LDA, +SOC	GGA, −SOC	GGA, +SOC
Dimer	FP-LMTO	7.57	7.56	8.06	8.04
Chain	FP-LMTO	7.75	7.75	8.53	8.22
Chain	WIEN	6.96		7.54	7.40
Hexagonal layer	WIEN	7.01		7.58	7.49
Square layer	WIEN	6.96		7.31	7.34
FCC crystal	WIEN	7.85		9.18	9.07
FCC crystal	LMTO-ASA	8.65			

Figure 1 shows the variation of the total energy as a function of the bond length. Also this figure confirms that spin–orbit couplings have only minor influences on the total-energy results. The figure shows also that the LDA calculations predict a larger binding energy than the GGA calculations, which is a common and well-known observation. The calculations were performed by considering an infinite chain of periodically repeated Xe_2 units that were placed perpendicular to the chain axis and with a repeat length of 200 au. Despite this long distance, it is interesting to notice that for the larger bond lengths (above ∼15 au) we found smaller differences when alternatively placing the Xe_2 units parallel to the chain axis. In the latter case the total-energy curve showed a slower convergence to a constant value without changing the other parts of the total-energy curve. It should, however, be stressed that the effects are so small that for most other systems with stronger interatomic interactions they will be unobservable. The result suggests that long-range interactions may have some small

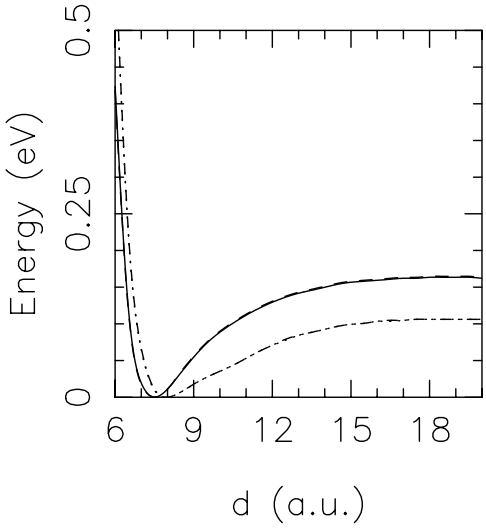

Figure 1. Variation in the total energy for the Xe_2 dimer as a function of bond length as obtained with (solid and dashed curves) LDA and (dotted and dash–dotted curves) GGA calculations without (solid and dotted) and with (dashed and dash–dotted) the inclusion of spin–orbit couplings. The results were obtained with the FP-LMTO method.

effects on the results of the WIEN programs for the monolayers and the chains, where we used interlayer and interchain distances of 30 and 15 au, respectively.

Figure 2 shows the variation of the single-particle energies for the Xe_2 dimer. Although the total energy appeared to converge more slowly as a function of the bond length d, these energies are largely converged to their isolated-atom limits for d larger than $\sim$12 au. These values are

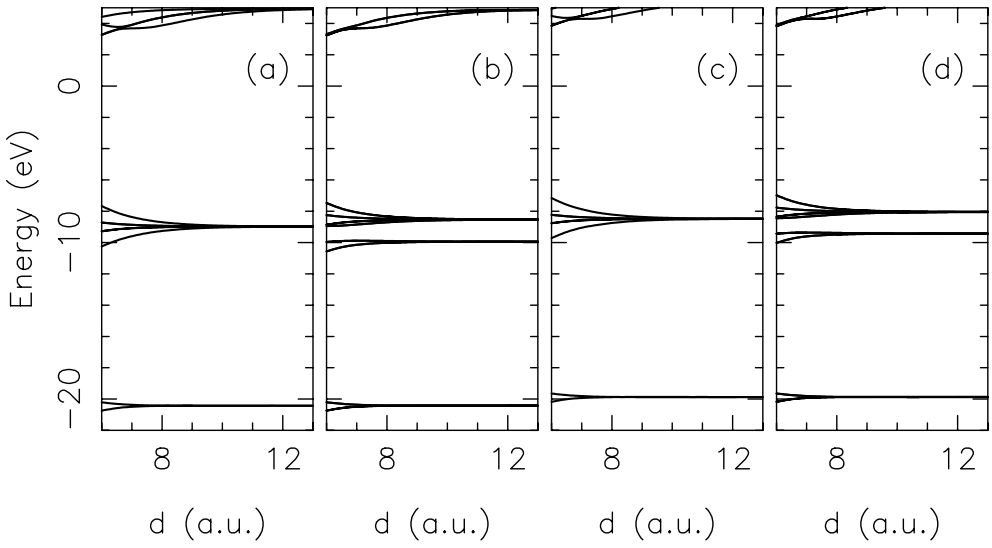

Figure 2. The single-particle energies for the Xe_2 dimer as functions of the bond length with ((a), (b)) LDA and ((c), (d)) GGA calculations without ((a), (c)) and with ((b), (d)) the inclusion of spin–orbit couplings. The results were obtained with the FP-LMTO method.

−20.43 and −8.98 eV for the LDA calculations and −19.87 and −8.48 eV for the GGA calculations. Since, in these calculations, only the spin–orbit couplings have been excluded, these values cannot be compared directly with those above for the isolated atom. Including the spin–orbit couplings led to −20.42, −9.94, and −8.53 eV for the LDA calculations and −19.87, −9.43, and −8.05 eV for the GGA calculations. Since these calculations use a finite basis set it is not obvious that the agreement with the results for the isolated atoms (the preceding subsection) is as good as it actually is.

3.3. The infinite chain

As for the dimer, the LDA calculations for the infinite, linear, periodic chain led to smaller optimized bond lengths than the GGA calculations (cf. table 1). Moreover, for the GGA calculations the inclusion of the spin–orbit couplings changed the optimized bond length of the GGA calculations somewhat, but, as seen in figure 3, the total-energy minimum is very shallow for the GGA calculations. In this figure it is also seen that passing from LDA to GGA reduces the binding energy, as for the dimer. Finally, table 1 suggests that the chain has a longer bond length than the dimer.

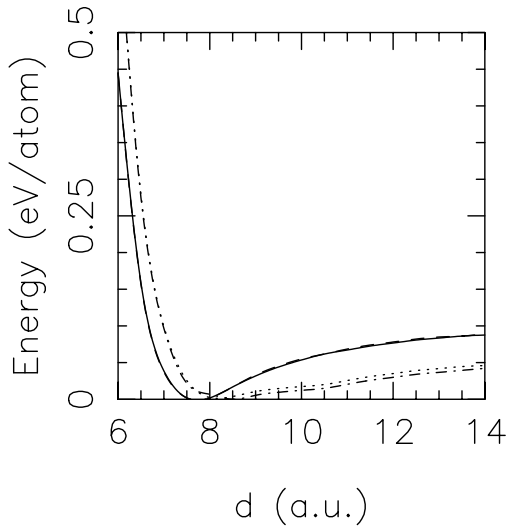

Figure 3. As figure 1, but for the linear chain.

With the WIEN programs we considered a hexagonal arrangement of parallel chains that were separated by 15 au. Taking the discussion of the preceding subsection into account, it may not surprise that the optimized bond length in this case differs markedly from that of the FP-LMTO calculations (cf. table 1).

Figure 4 shows the band structures for the four optimized structures of figure 3. Without the spin–orbit couplings, the valence bands split into one deep-lying σ-band from the 5s orbitals and a higher-lying manifold from the 5p orbitals consisting of a singly degenerate σ-band and a doubly degenerate π-band. As in figure 2, the inclusion of the spin–orbit couplings leads to a splitting of the p-derived bands into one lower-lying band and two higher-lying bands. Otherwise the bands show only little dispersion, as expected, and the largest differences between the different panels are due to spin–orbit couplings and to differences in the bond lengths.

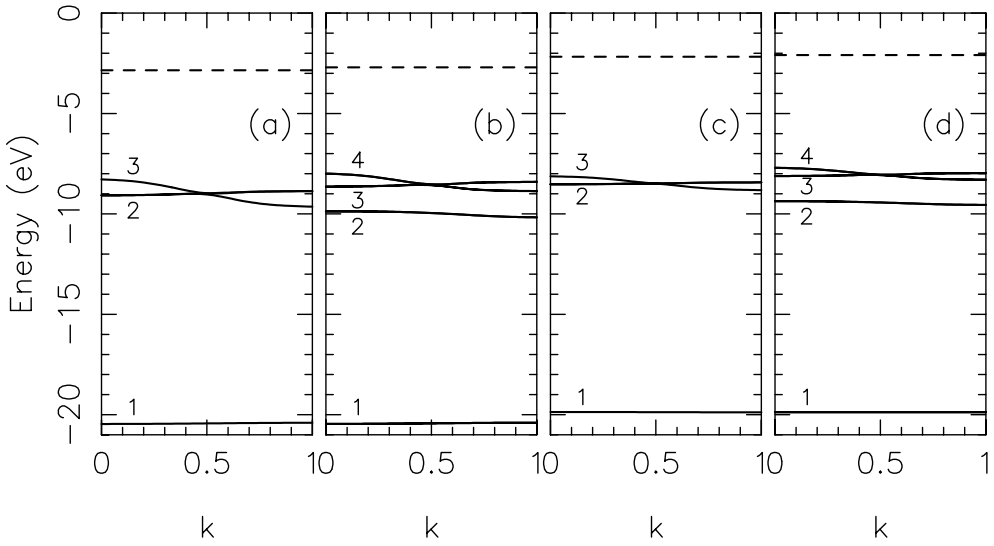

Figure 4. The band structures for the four optimized structures in figure 3. $k = 0$ and $k = 1$ represent the centre and the edge of the first Brillouin zone, respectively, and the dashed lines mark the Fermi level. The four different panels correspond to those of figure 2, and the results were obtained with the FP-LMTO method.

Since, however, the electronic bands are often used in experimentally characterizing the Xe systems deposited on some substrate, we shall discuss the variations of the band structures with bond lengths in some detail. First, in figure 5 we show the centre of the three (four)

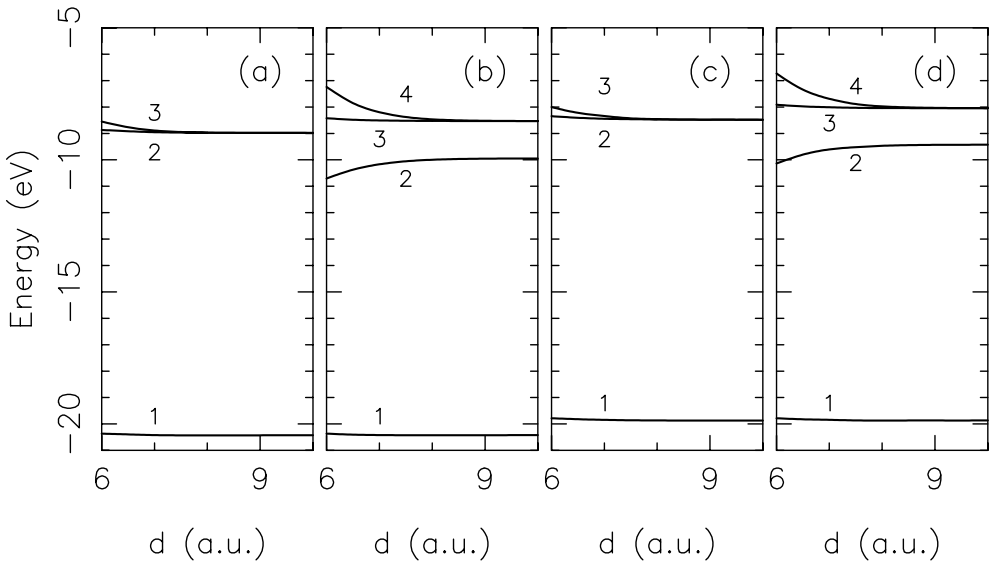

Figure 5. The centres of the bands as a function of the bond length for the same cases as in figure 4. The results were obtained with the FP-LMTO method, and the numbers refer to the bands of figure 4.

occupied bands without (with) spin–orbit couplings included. The fact that for bond lengths d above $\sim$10 au, the centres are, to a very good approximation, constants as functions of the bond lengths indicates that the Wannier functions that can be constructed for each band separately are then very close to being independent of d.

The bandwidths, figure 6, confirm this conclusion. The width of the energetically lowest band in figure 4 has a somewhat irregular behaviour and is even very close to 0 for $d \simeq 8.5$ au. This is due to an admixture of p functions with the otherwise mainly s-derived orbitals. But for d above 10 au the widths decrease monotonically as functions of d.

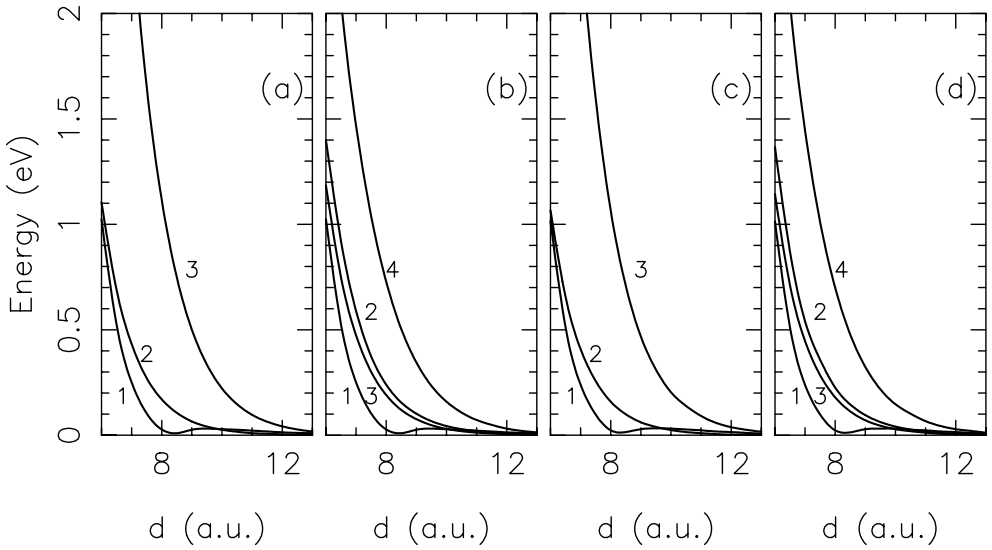

Figure 6. As figure 5, but for the bandwidths. The numbers refer to the bands of figure 4.

Assuming that we can describe the band structures for each band individually using a set of Wannier functions that are independent of d and that only nearest-neighbour interactions (t) need to be included, the band structures become

$$\epsilon_i(k) = \epsilon_i - 2t_i \cos(\pi k) \tag{5}$$

where i labels the bands and $k = 0$ and $k = 1$ are the centre and the edge of the first Brillouin zone as in figure 4. The width is then

$$w_i = 4t_i. \tag{6}$$

We used the results for $d \geqslant 10.0$ au in fitting

$$w_i \simeq \tilde{w}_i = a_i \mathrm{e}^{-b_i(d-d_0)} \tag{7}$$

or

$$w_i \simeq \tilde{w}_i = \alpha_i (d/d_0)^{-\beta_i}. \tag{8}$$

In all cases the fits were carried through by minimizing $\sum[\log(w_i) - \log(\tilde{w}_i)]^2$ where the sum runs over the different values of d, and the reference length d_0 was set equal to $d_0 = 10.0$ au.

The results of the fits are presented in table 2. In almost all cases (the exceptions are marked in the table) the fit of equation (7) is more accurate than that of equation (8) (on average, equation (7) led to bandwidths within 12% of the exact results, whereas those of equation (8) were within 14%). Moreover, when comparing the LDA and the GGA results

Table 2. Calculated parameters a_i, b_i, α_i, and β_i (cf. equations (7) and (8)) for the bandwidths of an infinite chain. 'LDA' and 'GGA' indicate which exchange–correlation functional is used, '+' and '−' under the heading SOC whether spin–orbit couplings have been included, and i refers to the bands of figures 4, 5, and 6. The asterisks mark those cases where the fit of equation (8) is better than that of equation (7).

LDA/GGA	SOC	i	a_i (meV)	b_i (au)	α_i (meV)	β_i
LDA	−	1	32	0.43	33	5.1
		2	28	1.05	29	12.0
		3	230	0.87	250	10.3
	+	1	34	0.50	35	5.9
		2	47	0.91	50	10.6
		3*	28	0.80	31	9.5
		4	165	0.83	178	9.9
GGA	−	1	36	0.50	37	5.9
		2*	20	0.78	22	9.3
		3	210	0.85	228	10.1
	+	1	34	0.48	36	5.6
		2	42	0.90	46	10.7
		3*	27	0.85	29	10.1
		4	152	0.83	165	9.9

there are only minor differences. Finally, the interactions between the Wannier orbitals of the energetically lowest band are more slowly decaying than those of the other occupied bands.

By comparing angle-resolved photoemission spectra for Xe chains deposited on different surfaces (thereby being able to vary the Xe–Xe intrachain distance), Widdra, Trischberger, and Henk [7] estimated that the width of the broadest band decays exponentially with a decay constant of 1.13 au that compares fairly well with the values of the table (although being some 25% larger). For a bond length of 8.26 au and for $k = 0$ they found bands at 4.1, 4.8, and 5.8 eV binding energy. We may, e.g., compare these values with those of figure 4(d) which gives binding energies of 9.4, 8.1, and 7.7 eV. Except for a constant shift (partly due to inaccuracies in the applied density-functional approximations and partly due to differences in the definition of the energy scale which for the experimental system is determined by the Pt substrate), the agreement is fair. However, the second value seems to show some difference between theory and experiment that might be due to interactions between the Xe chains and the substrate in the experiment. Also our calculated widths of 0.18, 0.15, and 0.60 eV are somewhat smaller (about 30%) than those found in the experimental study, which, once again, can be explained through substrate–Xe interactions. On the other hand, the experimental study was accompanied by theoretical KKR calculations on an isolated Xe chain. The band structures of these calculations were in excellent agreement with the experimental ones, although they disagree with both the FP-LMTO and the WIEN results of the present study.

In addition, the theoretical study of Henk and Feder [3] on a hexagonal Xe monolayer on Pt(111) predicted Xe states at roughly 6.0, 4.9, and 4.5 eV binding energy, which is in considerably better agreement with our theoretical values than the other results. This is also the case for the theoretical results of Hermann, Noffke, and Horn [2] on a free-standing hexagonal monolayer. They found for $\vec{k} = \vec{0}$ three levels with binding energies of 7.9, 6.6, and 6.2 eV.

In total this discussion suggests that the agreement between theory and experiment is not yet so perfect that we can exclude the possibility that substrate–Xe interactions modify the experimental results, and that they may be responsible for some discrepancies between experiment and theory.

The densities of states for the optimized structures are shown in figures 7(k)–7(m), and in table 3 we give the energy separation between and the widths of the various features in the figure. We see that the energy separation between the lower s-derived band and the higher p-derived bands is slightly larger than what we found above for the isolated atom, which, however, is in accordance with the results of figure 5. Also the widths of the bands in figures 7(k)–7(m) agree well with those of figure 6.

Table 3. Key quantities from the densities of states of figure 7. The quantities are ordered as in that figure and include for each panel the separation between the bands (first line) and the widths of the bands (second line). In those cases where spin–orbit couplings are included, more peaks occur in figure 7 just below the energy zero. Then, the first energy separation is between the lower band and the centre of all the upper bands, whereas the other separations are those between the band of interest and the uppermost occupied band. All quantities are given in eV.

	WIEN LDA, −SOC	WIEN GGA, −SOC	WIEN GGA, +SOC	LMTO-ASA LDA, −SOC
FCC crystal	11.58 0.49, 2.21	11.49 0.10, 0.72	11.49, 1.15 0.10, 0.40, 0.61	11.52 0.10, 1.13
Square layer	11.93 0.61, 2.55	11.83 0.34, 1.70	11.82, 1.25 0.41, 0.56, 1.44	
Hexagonal layer	12.02 0.72, 3.06	11.88 0.34, 1.88	11.99, 1.51 0.39, 0.65, 1.67	
Chain	11.96 0.34, 2.32	11.89 0.17, 1.34	11.85, 1.55, 0.58 0.19, 0.37, 0.20, 0.69	

Figure 6 shows that there are only minor differences between the LDA and the GGA bandwidths, and that the bandwidths, in general, increase with decreasing bond length and are, therefore, largest for the LDA-optimized structure. In this case (figure 7(k)) the bands are so wide that one can recognize the Van Hove singularities at the band edges. In all cases for the chains the narrow p-derived band (cf. figure 4) is also recognized. Finally, the p-derived bands in figure 7(m) split into three separated peaks in contrast to the bands of figure 4(d), which, however, may be due to the shorter bonds (cf. figure 5(d)).

3.4. The infinite monolayer

In order to treat a single monolayer we used the WIEN programs and studied square and hexagonal monolayers separated by 30.0 au. Optimizing the structures led to slightly smaller bond lengths for the former than for the latter (cf. table 1) although we cannot exclude the possibility that changes in the internal parameters of the calculations might change the bond lengths slightly. However, we consider studying this further as being beyond the scope of the present work.

The optimized bond lengths of these monolayers are very close to those found with the WIEN programs for the chains. We suggest that the experimental fact that the Xe_2 dimer and crystalline Xe have almost identical nearest-neighbour bond lengths indicates that the interatomic interactions are largely isotropic and short ranged, so other Xe systems (chains and monolayers, e.g.) should also have the same nearest-neighbour bond lengths.

In figures 7(e)–7(j) we show the densities of states for the different optimized structures, and table 3 contains the widths and energy separations.

When assuming that the monolayer is placed in the (x, y) plane, neglecting spin–orbit couplings, and only including nearest-neighbour interactions, the widths of the s- and p_z-derived bands should be twice as large for the square lattice as for the chain with the same

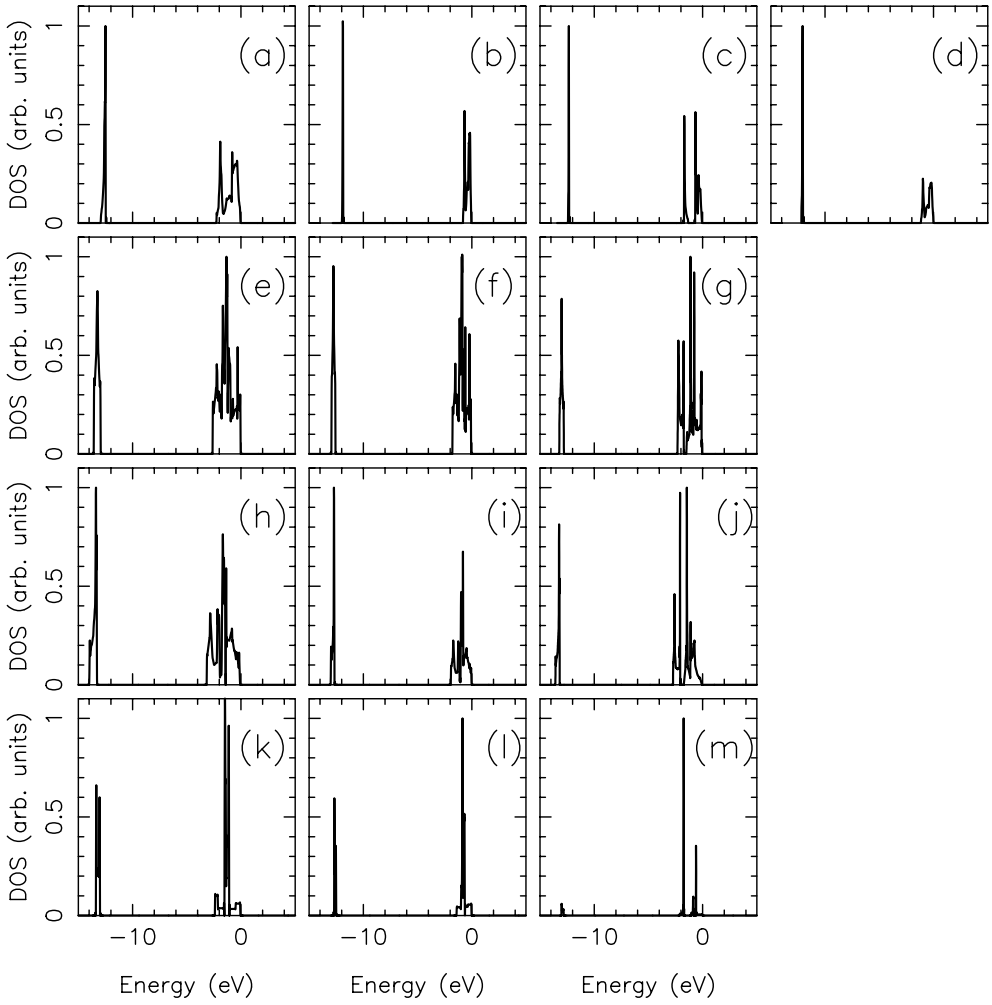

Figure 7. Densities of states for ((a)–(d)) crystalline FCC Xe, ((e)–(g)) a square monolayer of Xe, ((h)–(j)) a hexagonal monolayer of Xe, and ((k)–(m)) a single chain of Xe. The panels do not have the same ordinate scale and in each panel separately the energy zero is set at the top of the valence bands. The results of (d) have been obtained with the LMTO-ASA programs and the others with the WIEN programs. Panels (a), (d), (e), (h), and (k) have been found using a LDA, and the others with a GGA. Finally, panels (c), (g), (j), and (m) include spin–orbit couplings.

nearest-neighbour distance. Moreover, the bands formed by the p_x and p_y functions should have a total width of $4[(pp\sigma)+(pp\pi)]$ [35], whereas the width of the broad p band for the linear chain equals $4(pp\sigma)$. Here, $(pp\sigma)$ and $(pp\pi)$ are the hopping integrals for two p functions at different sites that are both either parallel or perpendicular to the interatomic vector. Since here $(pp\sigma) \gg (pp\pi)$, the widths for these bands should be very similar for the chains and the square monolayers. All of these predictions are confirmed in table 3.

For the hexagonal monolayer the widths of the s- and p_z-derived bands should be 1.125 times the widths for the square lattice, and also the widths of the (p_x, p_y) bands should be slightly larger. This is also confirmed by our calculations (see table 3).

Hermann, Noffke, and Horn [2] reported theoretical and experimental band structures for a

hexagonal monolayer of Xe (in the experimental study it was deposited on the Pd(100) surface) with nearest-neighbour bond lengths of 8.47 au. Figure 6 suggests that the bandwidths will be reduced roughly by a factor of 4 compared with the widths at our optimized structures (about 7 au). As in figure 7(j), the p-derived bands split into two separate features with a smaller gap in between, and they find a width of 0.38 eV for the lower band and a total width about 0.9 eV. These results are not in perfect agreement with our predictions, nor with their experimental results.

Finally, we mention that, in agreement with most of the results that we discussed in the preceding subsection for the chains, the density of states of the p-derived bands is split into two features with a separation of 1–1.5 eV. Whereas this was found in most theoretical studies, the experimental ones showed in some cases differences from this behaviour, as discussed in the preceding subsection.

3.5. The crystal

Experimentally, the lattice constant a of FCC Xe is 11.53 au [36] resulting in a nearest-neighbour distance of $d = a/\sqrt{2} = 8.15$ au. In their Hartree–Fock + correlation calculations, Rościszewski *et al* [32] found $d = 8.20$ au, in good agreement with the experimental value.

The WIEN calculations are not able to reproduce this value (cf. table 1). As is common for LDA calculations, the bonds are too strong and, in the present case, this leads to bonds that are too short. On the other hand, the GGA overcompensates this and leads to bonds that are too long. The difference between the optimized bond length of the chains and monolayers on the one hand and the crystal on the other is surprising. It may, however, be due to the presence of relatively close next-nearest neighbours for the crystal.

In the LMTO-ASA calculations further approximations to the potential are introduced and, as a consequence, the LDA calculations with these programs give bonds that are too long.

Figure 8 emphasizes these findings. With the WIEN programs, the LDA calculations give significantly larger binding energies than the GGA calculations independently of the inclusion of spin–orbit couplings. On the other hand, the LMTO-ASA calculations predict a markedly different behaviour of the interatomic interactions as a function of distance.

In one of the first theoretical studies of the bulk properties of Xe, Trickey, Green, and Averill [9] used the X_α approximation within density-functional theory as well as a muffin-tin approximation for the potential. Surprisingly, their calculations led to a very good agreement between theoretical and experimental lattice constants, which, however, may be merely fortuitous as their results for crystalline Ar and Kr show a worse agreement. The more recent LDA calculations by Caldwell *et al* [16] find a lattice constant 3–5% below the experimental value which is in excellent agreement with the present findings.

Figures 7(a)–7(d) show the densities of states for the different cases above, and table 3 contains some of the key quantities for them. The width of the s-derived band should in this case be four times that of the linear chain with the same bond length, which, however, is not found to be the case. Also the width of the p-derived bands should be larger than that of the linear chain with the same bond length. The fact that these predictions are not confirmed by the calculations suggests that more distant interactions (beyond nearest neighbours) are required and also that more subtle effects (hybridization) occur, so a discussion based on atomic-like orbitals is only approximately adequate. We add that the LMTO-ASA calculations that, after all, apply some further approximations lead to densities of states very similar to those from the other methods.

Bacalis, Papaconstantopoulos, and Pickett [37] calculated the band structures for crystalline Xe with the experimental lattice constant and using a LDA. They found that the uppermost

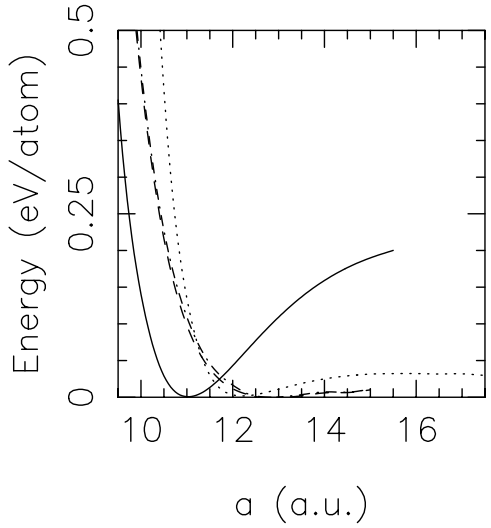

Figure 8. Variation in the total energy for crystalline FCC Xe as a function of the lattice constant. The solid curve shows results obtained with the WIEN programs and a LDA, whereas the dashed and dotted curves show similar results using a GGA. The LMTO-ASA method was used together with a LDA for the results shown by the dash–dotted curve. Only for the results shown by the dotted curve were spin–orbit couplings included.

valence bands have a width of 1.67 eV in good agreement with our results (cf. table 3) when taking the differences in the lattice constants into account. They found also that upon adding quasi-particle corrections this value was increased to 2.08 eV. The quasi-particle corrections may become important when making a detailed qualitative and quantitative comparison between experimental excitation energies and theoretical band structures. Their results suggest that these corrections mainly lead to an overall expansion of the band structures, which is also indicated by the related study of Chacham, Zhu, and Louie [15] on highly compressed xenon. The latter study shows also that relativistic effects are of only secondary importance, in agreement with our results. The quasi-particle results above imply that the experimentally derived band structures will be slightly broader than those that we have calculated here but that their shapes will stay unchanged. Finally, Halilov *et al* [38] have reported results of a combined experimental and theoretical study of a Xe(111) surface. Their calculated band structures give somewhat larger widths than those of the other studies, including ours.

4. Conclusions

The present study has shown that density-functional methods employing the currently popular LDA or GGA are not capable of describing the bond lengths of Xe-based systems. First of all, since the Xe_2 dimer and the crystalline FCC Xe, according to experiment, have essentially the same bond lengths, one would expect this also to be the case for chains and monolayers, which, however, is not found in the calculations. On the other hand, the results of the WIEN calculations indicate that there are differences between the crystalline systems and the others that might be due to next-nearest-neighbour interactions.

Furthermore, except for the LMTO-ASA calculations (that fail due to some extra approximations in the potential), the LDA calculations predict bonds that are too short and too strong, which is a general finding [39] and which has also been found for other inert-gas dimers [24].

Replacing the LDA with a GGA leads in general to longer and weaker bonds, once again in accord with general findings [24,39], but the accuracy is not necessarily increased. Moreover, in most cases spin–orbit couplings have only minor effects on the bond lengths, and most often they lead to a smaller reduction in these. Finally, our results on the Xe_2 dimer suggest that the calculated structural properties may depend very sensitively on how one approximates the system; i.e., when considering a system of repeated, essentially non-interacting, units, the inter-unit distance may have to be considerably larger than what usually is assumed. To the knowledge of the present author, only little is known about how different approximations employed by the different computational methods affect calculated structural properties, and due to its weak interatomic interactions Xe may be an extreme—and therefore well-suited—system for use in studying such effects.

Despite the problems in describing the correct structure, we believe that the electronic properties of these materials are accurately described (as is very often the case). We found that the distance dependences of the orbital interactions are best described with exponentials with decay constants in the range 0.5–1.0 au. For the experimentally produced quasi-1D and quasi-2D systems the interatomic distances are so large that the bandwidths are in the 0.01–0.1 eV range. When comparing our results with experimental photoelectron data some discrepancies were found, whereas the different theoretical methods used here gave mutually consistent results (the results were also consistent with those of most, but not all, other theoretical studies). This suggests that some substrate–Xe interactions are present, making a comparison between theory and experiment difficult. Similar effects (i.e., those beyond nearest Xe neighbours) may also be responsible for the differences between the bandwidths of crystalline Xe and those of the other systems.

Acknowledgments

The author is grateful to Karla Schmidt for useful discussions and to Fonds der Chemischen Industrie for very generous support. Moreover, this work was supported by the SFB 513 at the University of Konstanz.

References

[1] *Handbook of Chemistry and Physics* 1976 56th edn, ed R C Weast (Cleveland, OH: Chemical Rubber Company Press)
[2] Hermann K, Noffke J and Horn K 1980 *Phys. Rev.* B **22** 1022
[3] Henk J and Feder R 1994 *J. Phys.: Condens. Matter* **6** 1913
[4] Weinelt M, Trischberger P, Widdra W, Eberle K, Zebisch P, Gokhale S, Menzel D, Henk J, Feder R, Dröge H and Steinrück H-P 1995 *Phys. Rev.* B **52** R17 048
[5] Trischberger P, Dröge H, Gokhale S, Henk J, Steinrück H-P, Widdra W and Menzel D 1997 *Surf. Sci.* **377–379** 155
[6] Darling S B, Hanbicki A T, Pearl T P and Sibener S J 1999 *J. Phys. Chem.* B **103** 9805
[7] Widdra W, Trischberger P and Henk J 1999 *Phys. Rev.* B **60** R5161
[8] Wei S, Shi Z and Castleman A W Jr 1991 *J. Chem. Phys.* **94** 8604
[9] Trickey S B, Green F R Jr and Averill F W 1973 *Phys. Rev.* B **8** 4822
[10] Worth J P and Trickey S B 1979 *Phys. Rev.* B **19** 3310
[11] Ross M and McMahan A K 1980 *Phys. Rev.* B **21** 1658
[12] Ray A K, Trickey S B, Weidman R S and Kunz A B 1980 *Phys. Rev. Lett.* **45** 933
[13] Ray A K, Trickey S B and Kunz A B 1982 *Solid State Commun.* **41** 351
[14] Goettel K A, Eggert J H, Silvera I F and Moss W C 1989 *Phys. Rev. Lett.* **62** 665
[15] Chacham H, Zhu X and Louie S G 1992 *Phys. Rev.* B **46** 6688
[16] Caldwell W A, Nguyen J H, Pfrommer B G, Mauri F, Louie S G and Jeanloz R 1997 *Science* **277** 930
[17] Hohenberg P and Kohn W 1964 *Phys. Rev.* **136** B864

[18] Kohn W and Sham L J 1965 *Phys. Rev.* **140** A1133
[19] Desclaux J P 1969 *Comput. Phys. Commun.* **1** 216
[20] Blaha P, Schwarz K and Luiz J 1997 *WIEN97* Vienna University of Technology
This is an improved and updated Unix version of the original copyrighted WIEN code, which was published by Blaha P, Schwarz K, Sorantin P and Trickey S B 1990 *Comput. Phys. Commun.* **59** 399
[21] Springborg M and Andersen O K 1987 *J. Chem. Phys.* **87** 7125
[22] Springborg M, Calais J-L, Goscinski O and Eriksson L A 1991 *Phys. Rev.* B **44** 12 713
[23] Andersen O K 1975 *Phys. Rev.* B **12** 3060
[24] Pérez-Jordá J M and Becke A D 1995 *Chem. Phys. Lett.* **233** 134
[25] Hedin L and Lundqvist B I 1971 *J. Phys. C: Solid State Phys.* **4** 2064
[26] von Barth U and Hedin L 1972 *J. Phys. C: Solid State Phys.* **5** 1629
[27] Becke A D 1988 *Phys. Rev.* A **38** 3098
[28] Perdew J P and Wang Y 1992 *Phys. Rev.* B **45** 13 244
[29] Barker J A, Watts R O, Lee J K, Schafer T P and Lee Y T 1974 *J. Chem. Phys.* **61** 3081
[30] Wadt W R 1978 *J. Chem. Phys.* **68** 402
[31] Dehmer P M and Dehmer J L 1978 *J. Chem. Phys.* **68** 3462
[32] Rościszewski K, Paulus B, Fulde P and Stoll H 1999 *Phys. Rev.* B **60** 7905
[33] Nee J B, Kuo C T, Tseng H C and Wang S Y 2000 *Chem. Phys. Lett.* **318** 402
[34] Huzinaga S and Klobukowski M 1993 *Chem. Phys. Lett.* **212** 260
[35] Slater J C and Koster G F 1954 *Phys. Rev.* **94** 1498
[36] Sears D R and Klug H P 1962 *J. Chem. Phys.* **37** 3002
[37] Bacalis N V, Papaconstantopoulos D A and Pickett W E 1988 *Phys. Rev.* B **38** 6218
[38] Halilov S V, Tamura E, Gollisch H, Feder R, Kessler B, Müller N and Heinzmann U 1993 *J. Phys.: Condens. Matter* **5** 3851
[39] Perdew J P 1999 *Density Functional Theory: a Bridge between Chemistry and Physics* ed P Geerlings, F De Proft and W Langenaeker (Brussels: VUB Press)